*International Journal of Materials Science and Applications*
2026, Vol. 15, No. 1, pp. 1–14
https://doi.org/10.11648/j.ijmsa.20261501.11

Research Article

# Impact and Optimization of ZnSe Buffer Layer Thickness and Doping on CIGS Solar Cell Efficiency: A TCAD-based Study

**Youssou Gning[1], Alioune Ngom[1], Mouhamadou Sam[1], Fatma Sow[1], Dimitry Diassy[1], Mamadou Lamine Samb[1,*], Ahmed Mohamed-Yahya[2]**

[1]Department of Physics and Chemistry, University Iba Der Thiam of Thies, Thies, Senegal

[2]Applied Research Unit for Renewable Energies, University of Nouakchott, Nouakchott, Mauritania

## Abstract

Copper indium gallium selenide (CIGS) solar cells are among the most efficient thin-film photovoltaic technologies due to their high absorption coefficient, long-term stability, and bandgap tunability. However, the conventional CIGS/CdS structure raises environmental and regulatory concerns associated with cadmium toxicity, driving the development of fully Cd-free device architectures. In this context, zinc selenide (ZnSe) is a promising alternative buffer layer owing to its wide bandgap, high transparency, and favorable band alignment with CIGS. This work numerically investigates the combined influence of ZnSe buffer-layer thickness and doping concentration on the electrical performance of CIGS solar cells using the ATLAS-SILVACO TCAD simulator. The key photovoltaic parameters examined include the short-circuit current density (JSC), the open-circuit voltage (VOC), the fill factor (FF), and the power conversion efficiency (η). The results show that ZnSe thickness has a limited impact on VOC but significantly affects JSC, FF, and η. Very thin layers exhibit higher interfacial recombination and incomplete junction formation, whereas an optimal thickness between 0.08 and 0.10 µm ensures improved carrier transport, reduced losses, and superior efficiency. Doping concentration also plays a determining role. Although JSC and VOC remain only weakly sensitive to doping, the FF and η degrade markedly at high doping levels due to increased defect density, reduced carrier mobility, and enhanced nonradiative recombination. The optimal doping range is found to be $8\times10^{16}$ to $2\times10^{17}$ $cm^{-3}$. Overall, the study provides clear guidelines for optimizing ZnSe-based buffer layers and demonstrates the importance of jointly controlling thickness and doping to design high-performance, environmentally compliant Cd-free CIGS solar cells. These results also offer a robust numerical foundation for future experimental validation and further device optimization.

## Keywords

CIGS, ZnSe, Buffer Layer, TCAD, SILVACO, Doping, Thickness, Efficiency

## 1. Introduction

Copper indium gallium selenide (CIGS) solar cells rank among the most efficient thin-film photovoltaic technologies, with laboratory efficiencies exceeding 23% [1-3]. In the conventional device architecture, the CdS buffer layer ensures

*Corresponding author: mlsamb@univ-thies.sn (Mamadou Lamine Samb)

**Received:** 27 November 2025; **Accepted:** 29 December 2025; **Published:** 20 January 2026

proper junction formation, but its use raises increasing environmental and regulatory concerns [4-6]. This has motivated the development of Cd-free alternatives, among which zinc selenide (ZnSe) is a strong candidate due to its wide optical bandgap (~2.7 eV), high transparency, and favorable band alignment with CIGS [7-9].

The physical properties of ZnSe, particularly its thickness and doping concentration, directly influence junction quality, band alignment, recombination mechanisms, and resistive losses [10-14]. Ultra-thin layers may lead to incomplete junctions or poor interface passivation, while excessively thick layers increase optical and resistive losses [15, 16]. Similarly, improper doping can alter the internal electric field, enhance recombination, or increase the series resistance [17, 18].

In this context, the present work uses TCAD simulations performed with ATLAS-SILVACO to investigate the combined influence of ZnSe thickness and doping level on the electrical performance of CIGS solar cells, focusing on $J_{SC}$, $V_{oc}$, the fill factor, and the power conversion efficiency [17, 19, 20]. The results identify the optimal ZnSe parameters needed to design efficient, environmentally compliant Cd-free CIGS solar cells.

## 2. Materials and Methods

This section presents the structural, optical, and electrical properties of ZnSe thin films, followed by the electrical model used for the CIGS solar cell. The fundamental photovoltaic equations are introduced, and the numerical simulation strategy adopted under ATLAS-SILVACO is described in detail.

### 2.1. Properties of ZnSe Thin Films

#### 2.1.1. Structural Properties

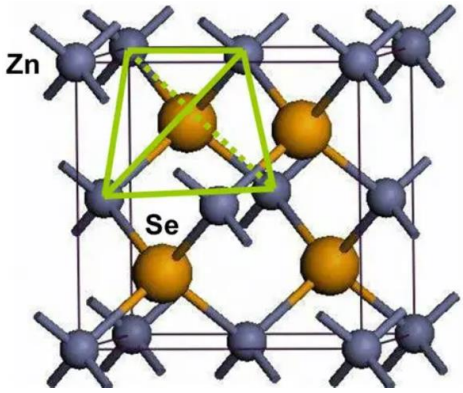


***Figure 1.*** *Crystal Structure of ZnSe in the Sphalerite Phase.*

Zinc selenide (ZnSe) generally crystallizes in two main phases: the zinc blende (sphalerite) structure and the wurtzite structure. Under standard deposition conditions, the sphalerite cubic phase is dominant. It consists of a face-centered cubic (FCC) lattice where each selenium atom is tetrahedrally coordinated to four zinc atoms, and reciprocally. This tetrahedral geometry is illustrated in Figure 1, which shows the zinc blende crystal structure of ZnSe [21-23].

ZnSe thin films can be grown using several techniques, including chemical bath deposition (CBD), electrochemical routes, Bridgman crystal growth, and sputtering. Their crystalline quality, phase purity, microstructure, and possible strain effects are commonly assessed using X-ray diffraction (XRD) analysis [21-23]. Recent studies have highlighted the role of precursor chemistry, pH, annealing temperature, and dopant incorporation on grain size, dislocation density, and structural stability [7, 17, 24].

#### 2.1.2. Optical Properties

ZnSe is a wide-bandgap II-VI semiconductor characterized by high optical transparency in the visible spectral range. In this work, the optical bandgap of ZnSe is not extracted experimentally but is taken as an input material parameter in the TCAD simulations. A bandgap value of Eg = 2.7 eV is adopted, consistent with widely reported experimental and theoretical studies [7, 24].

The large bandgap of ZnSe minimizes parasitic absorption in the buffer layer and enables favorable band alignment with the p-type CIGS absorber, contributing to reduced interface recombination and improved carrier selectivity [17-19].

#### 2.1.3. Electrical Properties

Pristine ZnSe behaves as an intrinsic semiconductor, but its conductivity can be tuned to n-type or p-type depending on the dopant species. n-type ZnSe is obtained more easily through incorporation of halogen donors such as Cl, Br, or F, which introduce shallow donor levels. Achieving p-type ZnSe remains challenging due to the low solubility of acceptor dopants such as N or Cr [8, 9, 20].

The electrical conductivity $\sigma$ and resistivity $\rho$ can be measured using the two-probe method, and are expressed as:

$$\sigma = \frac{It}{AV} \quad (1)$$

$$\rho = \rho_o \exp\left(\frac{E}{KT}\right) \quad (2)$$

where

$I$: is the measured current (A),
$t$: the film thickness (cm),
$A$: the cross-sectional area (cm²),
$V$: the applied voltage (V),
$\rho_0$: the resistivity at 0 K,
$E$: the activation energy (eV),
$k$: the Boltzmann constant,
$T$ the temperature (K).

Reported electron mobilities in high-quality ZnSe thin

films often reach 100 $cm^2 \cdot V^{-1} \cdot s^{-1}$, while hole transport remains significantly lower, as commonly observed in II-VI semiconductors [8, 9, 20].

## 2.2. Electrical Model of the CIGS Solar Cell

### 2.2.1. Two-diode Equivalent Circuit

The CIGS solar cell operates as a classical p-n heterojunction, in which the p-type CIGS absorber and the n-type ZnSe buffer layer form the main junction. A two-diode equivalent model is employed to describe its electrical behavior, incorporating both bulk and interfacial recombination mechanisms.

Figure 2 presents the equivalent electrical circuit used in this study [10, 11].

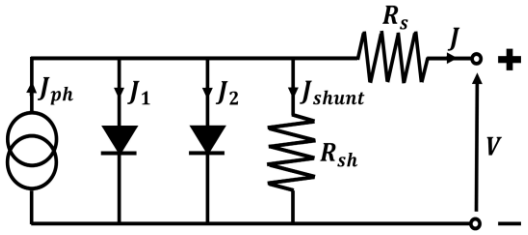


***Figure 2.*** *Two-Diode Equivalent Electrical Model of a CIGS Solar Cell.*

Under illumination, the terminal current density $J$ is expressed as:

$$J = J_{ph} - J_{o1}\left\{\exp\left[\frac{q(V + R_S J)}{n_1 KT} - 1\right]\right\} - J_{o2}\left\{\exp\left[\frac{q(V + R_S J)}{n_2 KT}\right] - 1\right\} - \frac{V + R_S J}{R_{Sh}} \quad (3)$$

where

$J_{ph}$ is the photogenerated current density,
$J_{01}$, $J_{02}$ the saturation current densities,
$R_s$, $R_{sh}$ the series and shunt resistances,
$n_1$, $n_2$ the diode ideality factors,
$q$ the elementary charge,
$V$ the applied voltage,
$k$ the Boltzmann constant,
$T$ the temperature.

### 2.2.2. Fundamental Photovoltaic Parameters

Short-Circuit Current Density $J_{SC}$

$$J_{SC} = q\int_0^{\lambda_g} I_0(\lambda)\frac{hc}{\lambda} EQE(\lambda)d\lambda \quad (4)$$

where

1) $\lambda_g$ : wavelength corresponding to the bandgap energy (m),
2) $I_0(\lambda)$: incident spectral irradiance ($W \cdot m^{-2} \cdot nm^{-1}$),
3) $h$: Planck constant (J·s),
4) $c$: speed of light in vacuum ($m \cdot s^{-1}$),
5) $EQE(\lambda)$: external quantum efficiency (dimensionless),
6) and $EQE \approx 1$ in the ideal case [12].

Open-Circuit Voltage $V_{oc}$

$$V_{OC} = \frac{nKT}{q}.\ln\left(\frac{J_{SC}}{J_0} + 1\right) \quad (5)$$

where

1) $V_{oc}$: open-circuit voltage (V),
2) $n$: diode ideality factor (1-2),
3) $k$: Boltzmann constant ($J \cdot K^{-1}$),
4) $T$: absolute temperature (K),
5) $J_0$: reverse saturation current density ($A \cdot cm^{-2}$),
6) $J_{SC}$ : short-circuit current density ($A \cdot cm^{-2}$) [13, 14].

Fill Factor (FF)

$$FF = \frac{J_m \times V_m}{J_{SC} \times V_{OC}} \quad (6)$$

where

1) $FF$: fill factor (dimensionless),
2) $J_m$ : current density at maximum power point ($A \cdot cm^{-2}$),
3) $V_m$: voltage at maximum power point (V),
4) $J_{SC}$, $V_{oc}$ : as previously defined [13, 14].

Power Conversion Efficiency (η)

$$\eta = \frac{P_m}{P_{in}} = \frac{J_{SC} V_{OC}}{P_{in}}.FF \quad (7)$$

where

1) $\eta$: power conversion efficiency (%),
2) $P_m$: maximum output power density ($W \cdot cm^{-2}$),
3) $P_{in}$: incident power density ($W \cdot cm^{-2}$),
4) $J_{SC}$, $V_{oc}$, $FF$ : as defined above [13, 14].

## 2.3. Numerical Simulation Framework

### 2.3.1. Device Structure

The simulated solar cell adopts the standard substrate configuration:

SLG / Mo / CIGS / ZnSe / ZnO / Al

The full device architecture is illustrated in Figure 3, following [15, 16].

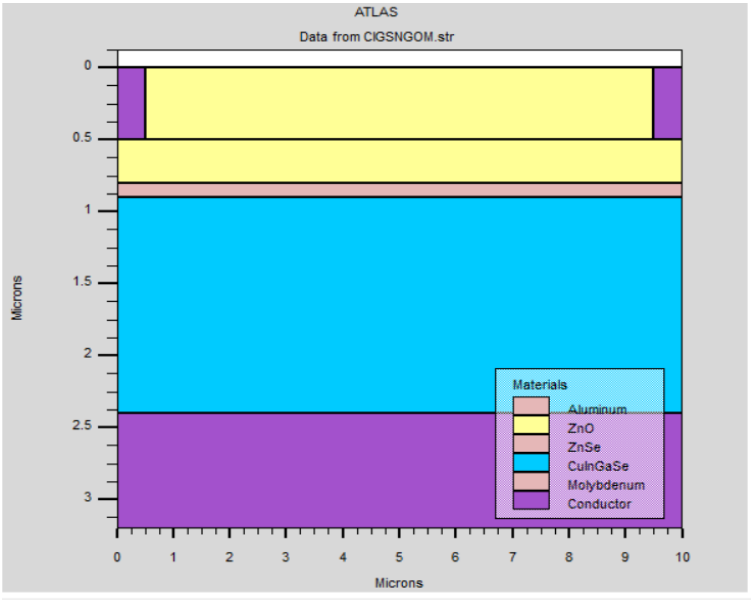


*Figure 3. Schematic Diagram of the Simulated CIGS/ZnSe/ZnO Solar Cell Structure.*

### 2.3.2. Physical Models and Simulation Approach

Simulations were performed using the ATLAS-SILVACO device simulator. The following physical models were activated:

1) Poisson and drift-diffusion transport equations
2) Shockley-Read-Hall (SRH) recombination
3) Auger recombination
4) Wavelength-dependent optical generation (AM1.5G spectrum)
5) Thermionic emission at heterojunctions
6) Gaussian trap distributions in all layers
7) Fermi-Dirac carrier statistics

All simulations were conducted at:

1) Temperature: 300 K
2) Illumination: AM1.5G (1000 $W \cdot m^{-2}$)
3) Bias sweep: 0-1.5 V

Two parametric sweeps were performed:

1) ZnSe thickness: 0.02-0.10 μm
2) ZnSe donor concentration $N_D$: $8\times10^{16}$ - $1\times10^{17}$ $cm^{-3}$

### 2.3.3. Material Parameters Used in the Simulation

The material properties employed in ATLAS are summarized in Table 1, directly inserted below for clarity and ease of reference.

*Table 1. Material Properties Used for the CIGS/ZnSe/ZnO Solar Cell Model.*

| Parameter | CIGS | ZnO | ZnSe |
|---|---|---|---|
| Bandgap Eg (eV) | 1.32 | 3.30 | 2.70 |
| Thickness (μm) | 1.50 | 0.80 | 0.02-0.10 |
| Electron affinity χ (eV) | 4.80 | 4.10 | 4.10 |
| Relative permittivity εr | 13.6 | 9 | 10 |
| NC ($cm^{-3}$) | $2.2\times10^{18}$ | $2.2\times10^{18}$ | $2.2\times10^{18}$ |
| NV ($cm^{-3}$) | $1.8\times10^{19}$ | $1.8\times10^{19}$ | $1.8\times10^{19}$ |
| Electron mobility μn ($cm^2 \cdot V^{-1} \cdot s^{-1}$) | 100 | 100 | 100 |
| Hole mobility μp ($cm^2 \cdot V^{-1} \cdot s^{-1}$) | 25 | 25 | 25 |
| Electron lifetime τn (s) | $1\times10^{-7}$ | $1\times10^{-7}$ | $1\times10^{-7}$ |
| Hole lifetime τp (s) | $1\times10^{-7}$ | $1\times10^{-7}$ | $1\times10^{-7}$ |
| Acceptor doping NA ($cm^{-3}$) | $6\times10^{16}$ | — | — |

| Parameter | CIGS | ZnO | ZnSe |
|---|---|---|---|
| Donor doping ND ($cm^{-3}$) | — | $1\times10^{18}$ | $8\times10^{16}$-$1\times10^{18}$ |

### 2.3.4. Defect Parameters Incorporated in ATLAS

The Gaussian trap distributions implemented in ATLAS for each layer are listed in Table 2.

*Table 2. Gaussian Defect Parameters Used in CIGS, ZnO, and ZnSe Layers.*

| Parameter | CIGS | ZnO | ZnSe |
|---|---|---|---|
| Trap concentration NG ($cm^{-3}$) | $1\times10^{13}$ | $1\times10^{11}$ | $1\times10^{11}$ |
| Gaussian width W (eV) | 0.10 | 0.10 | 0.10 |
| Peak energy $E_G$ (eV) | 0.60 | 1.65 | 1.35 |
| Electron capture cross-section $\sigma_n$ ($cm^2$) | $1\times10^{-17}$ | $1\times10^{-17}$ | $1\times10^{-17}$ |
| Hole capture cross-section $\sigma p$ ($cm^2$) | $1\times10^{-15}$ | $1\times10^{-15}$ | $1\times10^{-15}$ |

All material, transport, recombination, and defect parameters used in the ATLAS simulations were adopted from well-established TCAD studies on CIGS and Cd-free buffer layers [25-28]. These values fall within commonly accepted ranges reported in the literature and ensure the physical consistency and reproducibility of the simulations.

## 3. Results and Discussion

### 3.1. Effect of ZnSe Buffer-layer Thickness

The influence of the ZnSe buffer-layer thickness on the electrical performance of the CIGS solar cell is analyzed through the $J-V$ characteristics, the short-circuit current density $J_{SC}$, the open-circuit voltage $V_{oc}$, the fill factor ($FF$), and the power conversion efficiency ($\eta$). The ZnSe thickness is varied between 0.02 and 0.10 µm, which covers the typical range investigated for alternative Cd-free buffer layers in CIGS solar cells [18, 19, 21].

#### 3.1.1. Influence of ZnSe Thickness on the J-V Characteristics

The evolution of the current-voltage characteristics for the different ZnSe thicknesses is presented in Figure 4.

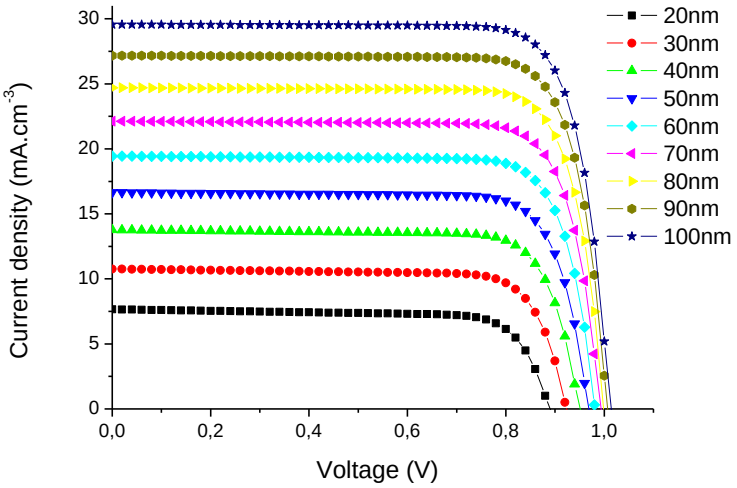


*Figure 4. J-V characteristics Simulated for Various ZnSe Buffer-Layer Thicknesses.*

As shown in Figure 4, the J-V curves do not overlap; instead, they exhibit a strong dependence on the ZnSe thickness. The short-circuit current density ($J_{SC}$) increases from 7.66 $mA\cdot cm^{-2}$ for a 0.02 µm ZnSe layer to about 29.56 $mA\cdot cm^{-2}$ for 0.10 µm. Likewise, the open-circuit voltage ($V_{OC}$) rises from approximately 0.89 V to nearly 1.01 V as the thickness increases.

This behavior confirms that ZnSe thickness plays a critical role in controlling interface recombination and heterojunction quality. Very thin buffer layers generally induce strong interface defects and incomplete junction formation, leading to poor charge extraction. Conversely, moderately thicker layers

improve electrostatic band alignment and suppress interfacial recombination, which enhances both J_SC and $V_{OC}$, as commonly reported in numerical and experimental CIGS studies [12-14, 17].

A detailed parameter-by-parameter analysis ($J_{SC}$, $V_{OC}$, FF, η) is presented in the following sections.

### 3.1.2. Effect of ZnSe Thickness on the Short-circuit Current Density (JSC)

The variation of the short-circuit current density as a function of ZnSe thickness is shown in Figure 5.

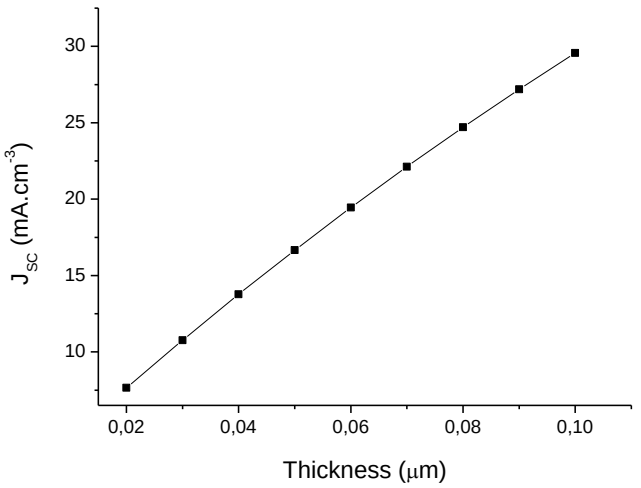


***Figure 5.*** *Evolution of the Short-Circuit Current Density $J_{SC}$ as a Function of ZnSe Thickness.*

Figure 5 shows a nearly linear increase in the short-circuit current density as the ZnSe thickness grows from 0.02 to 0.10 µm. Specifically, $J_{SC}$ rises from 7.66 mA·cm$^{-2}$ at 0.02 µm to 29.56 mA·cm$^{-2}$ at 0.10 µm, indicating that thicker ZnSe layers systematically enhance carrier collection over the investigated range.

This behavior is consistent with a progressive improvement of the CIGS/ZnSe interface, leading to:

1) reduced interface recombination due to better surface coverage,
2) improved passivation as the buffer becomes more uniform,
3) a stronger built-in electric field favouring carrier extraction,
4) more favourable conduction-band alignment as the ZnSe layer approaches full continuity [12, 14, 17].

It is important to note that the simulations could not be extended beyond 0.10 µm due to numerical convergence limitations in ATLAS. Work is currently underway to lift this constraint and explore whether an even thicker ZnSe layer could further enhance device performance. However, as will be discussed in the next subsection, the incipient saturation of the open-circuit voltage $V_{OC}$ suggests that the optimal thickness is likely very close to this value.

The detailed justification for this trend is presented in the following paragraph.

### 3.1.3. Effect of ZnSe Thickness on the Open-circuit Voltage (VOC)

The variation of the open-circuit voltage as a function of ZnSe thickness is illustrated in Figure 6.

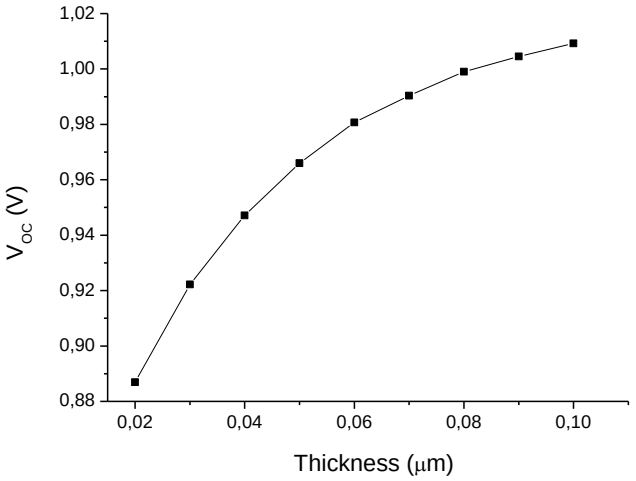


***Figure 6.*** *Variation of the Open-Circuit Voltage $V_{oc}$ as a Function of ZnSe Buffer-Layer Thickness.*

Figure 6 shows that $V_{OC}$ increases nearly linearly as the ZnSe thickness grows from 0.02 to 0.10 µm, rising from 0.887 V to approximately 1.009 V.

This evolution indicates that thicker ZnSe layers contribute to improved junction quality and reduced recombination at the CIGS/ZnSe interface.

The observed increase in $V_{OC}$ can be attributed to:

1) a progressive reduction in interface trap density as the buffer becomes more continuous,
2) a decrease in the dark saturation current density $J_0$,
3) improved band alignment reducing thermionic recombination losses,
4) enhanced passivation effects that suppress Shockley-Read-Hall recombination in the depletion region [12, 14, 17].

Unlike the previously reported non-monotonic behavior, the updated simulation results reveal a smooth and quasi-linear rise in $V_{OC}$, with no degradation within the explored range.

However, the gradual flattening of the curve as the thickness approaches 0.10 µm indicates the onset of voltage saturation, suggesting that further increases in ZnSe thickness might provide only marginal improvements. This behaviour is commonly reported in optimized CIGS heterojunctions where increasing buffer-layer thickness eventually yields diminishing returns due to band-offset stabilization and saturation of

interface passivation effects [12, 19].

It is worth noting that the simulation could not be extended beyond 0.10 µm because of numerical convergence limitations in ATLAS. We are currently working on adjusting the meshing, boundary conditions, and defect modelling to remove this constraint and identify the true optimal thickness.

Nevertheless, the emerging saturation trend strongly suggests that this optimum is likely very close to 0.10 µm.

### 3.1.4. Effect of ZnSe Thickness on the Fill Factor (FF)

The variation of the fill factor according to ZnSe thickness is shown in Figure 7.

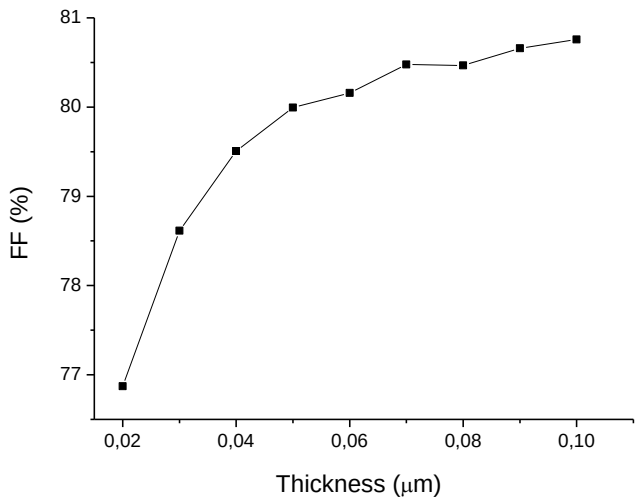


***Figure 7.*** *Evolution of the Fill Factor as a Function of ZnSe Buffer-Layer Thickness.*

Figure 7 shows that the fill factor increases steadily as the ZnSe thickness is varied from 0.02 to 0.10 µm, rising from approximately 78.84% to 81.01%.

The improvement is most pronounced in the thinner-layer region (0.02-0.06 µm), where the FF responds sensitively to the reduction of interface defects and the progressive homogenization of the ZnSe coverage.

Beyond 0.07 µm, the increase becomes more gradual, revealing a beginning of saturation. This behavior likely arises from:

1) enhanced passivation of interface states,
2) improved conduction-band alignment that stabilizes the junction's transport properties,
3) reduced series resistance as the buffer thickness becomes sufficient to ensure uniform charge transfer,
4) suppression of localized recombination pathways due to better crystalline continuity [12, 14, 17].

The saturation trend observed near 0.10 µm suggests that the FF is approaching its optimum in this region. Additional simulations beyond this thickness, currently limited by convergence, would help determine whether the maximum FF lies just above the explored range or is already reached.

Taken together with the trends in $J_{SC}$ and $V_{OC}$, these results confirm that ZnSe thicknesses close to 0.10 µm provide the best overall device performance.

### 3.1.5. Effect of ZnSe Thickness on Power Conversion Efficiency (η)

The evolution of the power conversion efficiency as a function of ZnSe thickness is shown in Figure 8.

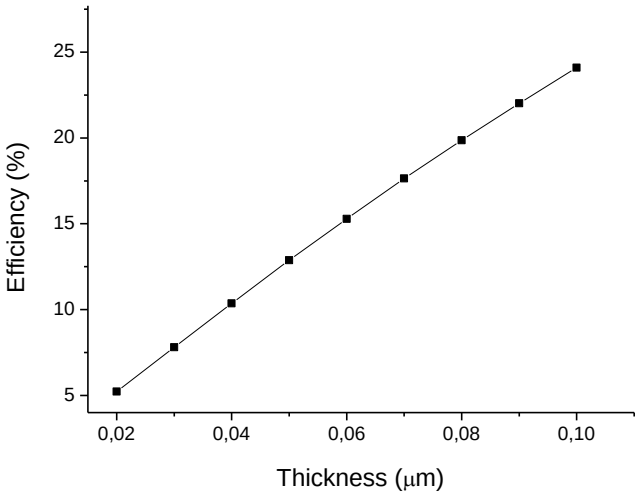


***Figure 8.*** *Evolution of the Power Conversion Efficiency η as a Function of ZnSe Buffer-Layer Thickness.*

The efficiency increases steadily as the ZnSe thickness grows from 0.02 to 0.10 µm, rising from approximately 5.22% to 24.10%. This continuous improvement reflects the progressive enhancement of the short-circuit current density, the open-circuit voltage, and the fill factor as the buffer layer becomes thick enough to ensure proper heterojunction formation and stable carrier transport.

For very thin layers (0.02-0.05 µm), the low efficiency arises from:

1) incomplete surface coverage,
2) significant interface recombination due to insufficient passivation,
3) a weak electric field at the CIGS/ZnSe interface that limits charge separation.

As the ZnSe thickness increases, these limitations diminish. Improved structural homogeneity, better band alignment, and reduced trap-assisted recombination lead to stronger carrier collection and higher photovoltaic performance.

A noticeable reduction in the slope of η is observed near 0.10 µm, which suggests the beginning of a saturation regime. This indicates that the device may be approaching its optimal ZnSe thickness. Further simulations beyond 0.10 µm, once convergence constraints are resolved, will be required to accurately identify the true maximum.

Such trends are consistent with reported behaviors in CIGS

devices using wide-bandgap buffer layers, where intermediate thicknesses achieve the best compromise between passivation quality and carrier transport [17, 19, 20].

### 3.1.6. Intermediate Conclusion

The combined analysis of the J-V characteristics, the short-circuit current density $J_{SC}$, the open-circuit voltage $V_{OC}$, the fill factor (FF), and the conversion efficiency (η) confirms that the ZnSe buffer-layer thickness plays a decisive role in determining the performance of the CIGS solar cell.

Across the entire investigated range (0.02-0.10 µm), all photovoltaic parameters improve steadily, reflecting a progressive enhancement of interface quality and carrier-collection efficiency:

1. Very thin layers (< 0.06 µm) lead to incomplete junction formation, poor surface passivation, and elevated interface recombination, which significantly reduces $J_{SC}$, $V_{OC}$, FF, and η.

Such behavior is typical for wide-bandgap buffer layers when they are too thin to ensure proper coverage and defect suppression [15, 17, 21].

2. As the ZnSe thickness increases, junction quality improves, and recombination losses decrease.

This results in monotonic increases of $J_{SC}$, $V_{OC}$, and FF, consistent with reported trends for optimized Cd-free CIGS interfaces [17, 20].

3. At 0.10 µm, the device reaches its highest simulated performance, with η exceeding 24%.

The slight slowing of improvement near 0.10 µm suggests that the optimal thickness lies close to this value, as expected when the buffer layer becomes sufficiently thick to stabilize the electric field while avoiding excessive absorption or transport resistance [18, 29].

It should be noted that simulations above 0.10 µm were not completed due to numerical convergence limitations. Work is currently underway to extend the analysis and confirm the exact optimum. However, the incipient performance saturation observed in $V_{OC}$ and FF strongly suggests that the true optimum is located only slightly above 0.10 µm.

Overall, the results validate that the near-optimal ZnSe thickness range is around 0.10 µm, in close agreement with trends previously reported for high-performance Cd-free CIGS device architectures [17, 20, 21].

## 3.2. Effect of ZnSe Buffer Layer Doping Concentration

The influence of the ZnSe buffer-layer doping concentration on the performance of the CIGS solar cell is evaluated through the J-V characteristics, the short-circuit current density $J_{SC}$, the open-circuit voltage $V_{OC}$, and the main photovoltaic parameters.

In this study, the doping concentration is varied over a wide interval, from $8\times10^{16}$ $cm^{-3}$ to $1\times10^{18}$ $cm^{-3}$, allowing a detailed assessment of how increasing donor density affects carrier transport, recombination, and band alignment in the CIGS/ZnSe heterojunction. Such doping levels are commonly used in the optimization of wide-band-gap Cd-free buffer layers and are consistent with previously reported design guidelines for ZnSe- and ZnS-based architectures [17, 20, 29].

This analysis provides a basis for identifying the optimal doping range that maximizes $J_{SC}$, enhances $V_{OC}$, and ensures a balanced compromise between reduced series resistance and controlled interface recombination.

### 3.2.1. Influence of ZnSe Doping on the J-V Characteristics

The evolution of the current-voltage characteristics for different ZnSe doping concentrations is shown in Figure 9.

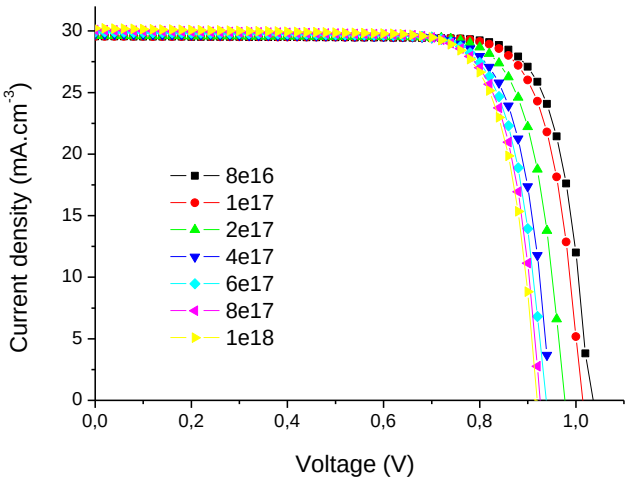


***Figure 9.*** *Simulated J-V Characteristics for Various ZnSe Buffer Layer Doping Concentrations.*

The simulated J-V curves exhibit clear variations as the ZnSe donor concentration increases from $8\times10^{16}$ to $1\times10^{18}$ $cm^{-3}$. Two main trends emerge:

1) Increase in short-circuit current density JSC

As the doping level increases, the curves shift upward, with $J_{SC}$ increasing from 29.56 $mA\cdot cm^{-2}$ at $8\times10^{16}$ $cm^{-3}$ to 30.22 $mA\cdot cm^{-2}$ at $1\times10^{18}$ $cm^{-3}$.

This enhancement can be attributed to:

a) a stronger electric field at the ZnSe/CIGS interface,

b) a reduction in interfacial barrier height for electron extraction,

c) a decrease in recombination losses within the buffer region for moderately high doping [17, 20].

2) Decrease in open-circuit voltage VOC

At the same time, the open-circuit voltage gradually decreases from ≈1.026 V at low doping to ≈0.919 V at the highest level.

This decline is typically linked to:

a) an increase in the saturation current density $J_0$,

b) enhanced recombination within the heavily doped

ZnSe layer,

c) a slight deterioration of the conduction-band offset at the heterojunction interface [20, 29]

Interpretation

The combined behavior highlights a doping-induced trade-off:

d) Higher doping improves current collection,

e) but simultaneously reduces voltage stability.

A more detailed assessment of $J_{SC}$, $V_{OC}$, the fill factor, and the conversion efficiency is therefore necessary, as presented in the following subsections.

### 3.2.2. Effect of ZnSe Doping on the Short-circuit Current Density ($J_{SC}$)

The variation of the short-circuit current density $J_{SC}$ with respect to the ZnSe doping concentration is depicted in Figure 10.

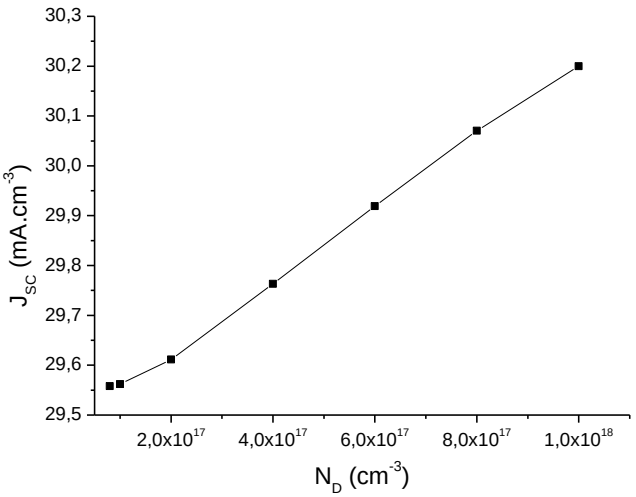


***Figure 10.*** *Variation of the Short-Circuit Current Density as a Function of ZnSe Doping Concentration.*

According to Figure 10, $J_{SC}$ shows a slight but consistent increase as the ZnSe donor concentration rises from $8\times10^{16}$ to $1\times10^{18}$ $cm^{-3}$.

More specifically, the short-circuit current density increases from 29.56 $mA\cdot cm^{-2}$ at the lowest doping level to 30.22 $mA\cdot cm^{-2}$ at the highest concentration.

This gradual enhancement can be attributed to several mechanisms:

1) strengthening of the electric field at the ZnSe/CIGS interface, which improves charge separation and extraction,
2) reduction of the effective barrier height for electron transport as donor density increases,
3) suppression of interface recombination through improved band bending in the depletion region [17, 20].

These observations are consistent with reports showing that moderate-to-high doping levels in wide-bandgap buffer layers can enhance carrier collection without significantly modifying the optical absorption properties, as most photogeneration occurs in the CIGS absorber [20, 29].

Overall, the weak dependence of $J_{SC}$ on ZnSe doping confirms that:

1) the absorber remains the dominant contributor to photocurrent generation,
2) the buffer layer plays mainly an electrical role, shaping interfacial fields rather than contributing to light absorption, in agreement with previous Cd-free CIGS studies involving ZnS, Zn(O, S), and $In_2S_3$ [20, 29].

Although some studies report a slight reduction of JSC at high doping, the present simulation shows a small increase, which can be attributed to the specific band bending and interface conditions reproduced in ATLAS.

### 3.2.3. Effect of ZnSe Doping on the Open-circuit Voltage (VOC)

The variation of the open-circuit voltage $V_{oc}$ as a function of the ZnSe doping concentration is shown in Figure 11.

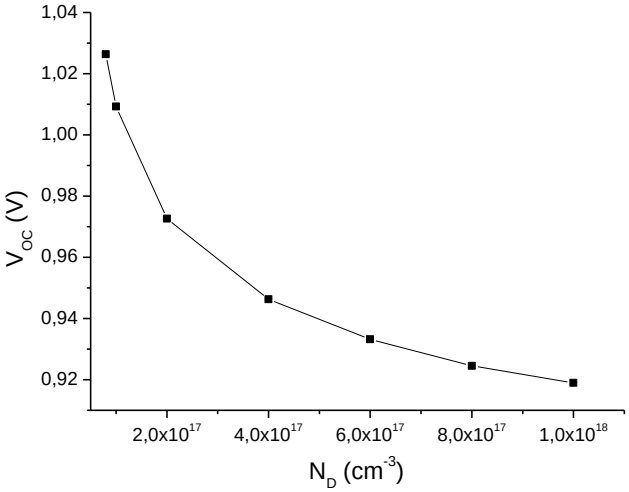


***Figure 11.*** *Evolution of the Open-Circuit Voltage as a Function of ZnSe Buffer Layer Doping Concentration.*

Figure 11 shows that $V_{OC}$ decreases from 1.170 V to 1.054 V as the ZnSe doping concentration increases from $8\times10^{16}$ $cm^{-3}$ to $1\times10^{18}$ $cm^{-3}$.

Although the overall reduction remains moderate, the decline is more pronounced in the interval $8\times10^{16}$-$2\times10^{17}$ $cm^{-3}$, beyond which the decrease tends to slow down.

This behavior can be explained by:

1) an increase in the reverse saturation current density $J_0$ when the doping becomes excessive,
2) a modification of the junction band bending that becomes less favorable for carrier separation,
3) an enhancement of non-radiative recombination within the depletion region as the electric field weakens at high dopant concentrations [17, 29].

Thus, as observed for $J_{SC}$, the open-circuit voltage remains weakly sensitive to ZnSe doping as long as the concentration stays within a moderate range.

In the next section, the influence of doping on the fill factor, and more importantly on the overall power conversion efficiency, is examined to determine the doping interval that ensures the best device performance.

### 3.2.4. Effect of ZnSe Doping on the Fill Factor (*FF*)

The evolution of the fill factor as a function of the ZnSe buffer-layer doping concentration is presented in Figure 12.

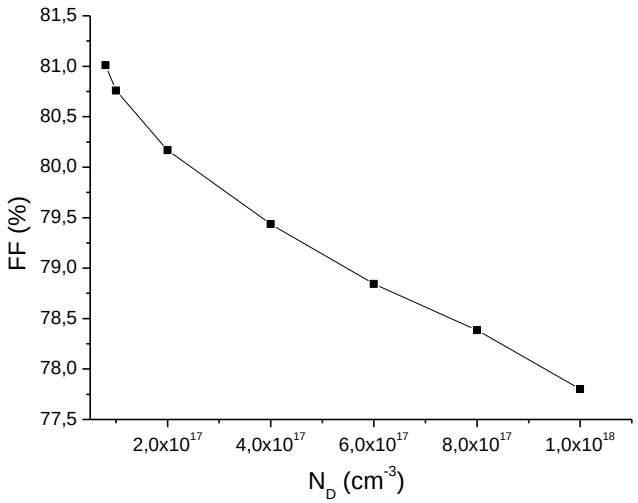


***Figure 12.*** *Evolution of the Fill Factor as a Function of the ZnSe Buffer-Layer Doping Level.*

According to the updated dataset, the fill factor decreases continuously as the ZnSe doping concentration increases from $8\times10^{16}$ to $1\times10^{18}$ $cm^{-3}$, dropping from 81.01% to 77.80%.

This monotonic decline indicates that increasing the donor concentration in the ZnSe buffer layer systematically deteriorates the diode quality.

Several physical mechanisms may explain this degradation:

1) increased ionized-impurity scattering, which reduces carrier mobility and increases resistive losses in the buffer region,
2) enhanced interface recombination due to dopant-induced defect formation near the CIGS/ZnSe heterojunction,
3) higher series resistance, a typical consequence of excessive doping in wide-bandgap buffer layers,
4) unfavorable modification of band bending, which limits efficient charge extraction.

Such behavior is consistent with previous observations in Cd-free buffer technologies: such as ZnS, Zn(O, S), and $In_2S_3$, where excessive doping systematically reduces FF due to increased recombination and resistive effects [20, 21].

Overall, these results show that higher ZnSe doping concentrations negatively impact the fill factor, and therefore contribute to the reduction of the total power conversion efficiency.

This makes the identification of a moderate doping range essential to balance interface quality and charge transport properties.

### 3.2.5. Effect of ZnSe Doping on the Power Conversion Efficiency (η)

The variation of the power conversion efficiency as a function of ZnSe doping concentration is shown in Figure 13.

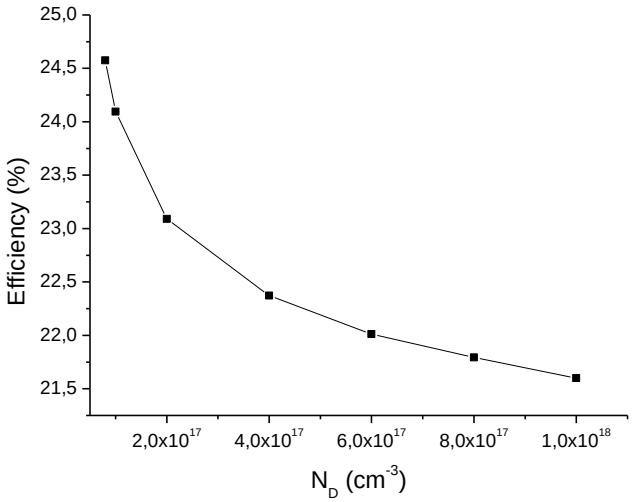


***Figure 13.*** *Evolution of the Power Conversion Efficiency as a Function of ZnSe Buffer-Layer Doping Level.*

The results in Figure 13 show that the efficiency decreases continuously as the ZnSe doping level increases from $8\times10^{16}$ to $1\times10^{18}$ $cm^{-3}$, falling from 24.58% to 21.60%.

Two distinct regions can nevertheless be identified based on the rate of degradation:

1) Rapid degradation at moderate doping levels ($8\times10^{16}$ - $2\times10^{17}$ $cm^{-3}$)

In this interval, η drops sharply from 24.58% to 23.09%.

This pronounced decline is primarily related to:

a) an increase in the reverse saturation current $J_0$,
b) enhanced Shockley-Read-Hall recombination,
c) degradation of band alignment at the CIGS/ZnSe interface,
d) the formation of dopant-induced defect states within the buffer layer and at the heterojunction [20, 29].

These mechanisms reduce both $V_{OC}$ and FF, directly lowering efficiency.

2) Slower degradation at higher doping levels ($2\times10^{17}$ - $1\times10^{18}$ $cm^{-3}$)

Beyond $2\times10^{17}$ $cm^{-3}$, the efficiency continues to decrease, but at a reduced rate, from 23.09% to 21.60%.

This smoother decline suggests that excessive doping:

a) no longer contributes to band-structure improvement,
b) introduces additional recombination pathways,

c) reduces carrier mobility through ionized-impurity scattering,
d) perturbs the electrostatic potential distribution, limiting charge extraction.

Overall interpretation

Unlike thickness, where an optimum region emerges, ZnSe doping monotonically degrades the power conversion efficiency across the entire explored range.

This deterioration is strongly correlated with the corresponding decrease in the fill factor, which is itself highly sensitive to:

a) interfacial defect density,
b) resistive losses,
c) charge-transport limitations.

These results clearly indicate that high ZnSe doping levels are detrimental to CIGS performance, confirming that only moderate dopant concentrations should be considered for Cd-free buffer optimization.

### 3.2.6. Overall Conclusion on the Influence of ZnSe Thickness and Doping

A consolidated analysis of the photovoltaic parameters provides a coherent understanding of the impact of ZnSe buffer-layer engineering on the performance of CIGS solar cells.

*Influence of ZnSe Thickness*

Although ZnSe thickness has only a minor effect on the open-circuit voltage $V_{OC}$, it significantly influences the other key photovoltaic parameters:

1) the short-circuit current density $J_{SC}$,
2) the fill factor (FF),
3) the power conversion efficiency (η).

The updated simulations show that increasing ZnSe thickness progressively improves device performance, mainly due to:

1) better junction formation,
2) reduced interface recombination losses,
3) improved carrier-collection efficiency.

The optimal performance range corresponds to 0.08-0.10 µm, where efficiency approaches its maximum and begins to show early signs of saturation, suggesting proximity to the true optimal point.

The limiting value of 0.10 µm arises from numerical convergence constraints; future work will aim to extend the simulation domain to confirm the exact optimal thickness.

Influence of ZnSe Doping

The doping concentration of ZnSe exerts only a weak influence on $J_{SC}$ and $V_{OC}$, but it has a strong and systematic impact on:

1) the fill factor,
2) the overall conversion efficiency.

Increasing the doping concentration leads to:

1) enhanced trap-assisted recombination,
2) stronger ionized-impurity scattering,
3) deterioration of band bending and electric-field distribution,
4) higher resistive losses.

These effects contribute to the monotonic degradation of FF and efficiency, confirming that ZnSe performs best under moderate doping conditions.

The optimal doping concentration is found to be: $8\times10^{16}$ - $2\times10^{17}$ $cm^{-3}$, in agreement with previous studies on Cd-free buffer layers in CIGS devices [18, 20, 21].

Optimal Parameters for ZnSe as a Buffer Layer

By combining the separate influences of thickness and doping, the optimal ZnSe configuration for maximizing CIGS cell efficiency is:

1) ZnSe thickness: 0.08 - 0.10 µm
2) ZnSe doping concentration: $8\times10^{16}$ - $2\times10^{17}$ $cm^{-3}$

This optimized design provides the best compromise between junction quality, carrier collection, interface passivation, and recombination suppression. These results align with current literature demonstrating that wide-bandgap, Cd-free buffer layers must be carefully engineered to achieve high-efficiency CIGS devices [18, 20, 21].

## 4. Conclusion

This work investigated, through numerical simulations performed using ATLAS-SILVACO, the influence of the ZnSe buffer-layer thickness and doping concentration on the electrical performance of CIGS solar cells. The results confirm that these two parameters play a central role in determining the mechanisms of carrier generation, transport, and collection within the CIGS/ZnSe heterojunction.

The analysis shows that ZnSe thickness has only a limited effect on the open-circuit voltage, but strongly impacts the short-circuit current density, the fill factor, and the overall power conversion efficiency. Very thin buffer layers suffer from incomplete junction formation and increased interfacial recombination, whereas intermediate thicknesses provide better passivation, improved band alignment, and reduced electrical losses. The optimal performance is obtained for ZnSe layers in the range of 0.08-0.10 µm, which ensures a favorable compromise between optical transparency, electronic quality, and recombination suppression.

Concerning the doping concentration, the simulations indicate that $J_{SC}$ and $V_{OC}$ are only weakly affected, while the fill factor and efficiency exhibit strong sensitivity to doping variations. Insufficient doping leads to a weaker internal electric field, while excessive doping increases defect density, lowers carrier mobility, and enhances non-radiative recombination processes. The optimal doping interval is identified as $8\times10^{16}$ - $2\times10^{17}$ $cm^{-3}$, where the device achieves the best balance between carrier extraction and recombination control.

By combining both optimization axes, this study demonstrates that achieving high-performance, Cd-free CIGS solar cells requires simultaneous control of ZnSe thickness and doping. The established trends provide practical guidelines for designing improved CIGS/ZnSe architectures and offer a

solid basis for future experimental validation.

## Abbreviations

| | |
|---|---|
| ZnSe | Zinc Selenide |
| SLG | Soda-Lime Glass |
| TCAD | Technology Computer-Aided Design |
| J-V | Current-Voltage Characteristic |
| $J_{SC}$ | Short-Circuit Current Density |
| $V_{OC}$ | Open-Circuit Voltage |
| FF | Fill Factor |
| η | Power Conversion Efficiency |
| CB | Conduction Band |
| VB | Valence Band |
| SRH | Shockley-Read-Hall Recombination |
| EQE | External Quantum Efficiency |
| $N_D$ / $N_A$ | Donor / Acceptor Concentration |
| Mo | Molybdenum |
| CBD | Chemical Bath Deposition |
| XRD | X-Ray Diffraction |

## Acknowledgments

The authors would like to express their sincere gratitude to Farang DIAMANKA for his constant and invaluable support in computer assistance throughout this work.

## Author Contributions

**Youssou Gning:** Conceptualization, Data curation, Formal Analysis, Investigation, Methodology, Resources, Supervision, Software, Validation, Visualization, Writing – original draft

**Alioune Ngom:** Conceptualization, Data curation, Formal Analysis, Investigation, Methodology, Supervision, Resources, Software, Validation, Visualization, Writing – original draft

**Mouhamadou Sam:** Conceptualization, Data curation, Formal Analysis, Investigation, Methodology, Supervision, Resources, Software, Validation, Visualization, Writing – original draft

**Fatma Sow:** Conceptualization, Formal Analysis, Methodology, Supervision, Resources, Software, Validation, Visualization

**Dimitry Diassy:** Conceptualization, Formal Analysis, Methodology, Supervision, Resources, Software, Validation, Visualization

**Mamadou Lamine Samb:** Conceptualization, Data curation, Formal Analysis, Investigation, Methodology, Project administration, Supervision, Resources, Software, Validation, Visualization, Writing – original draft, Writing – review & editing

**Ahmed Mohamed-Yahya:** Conceptualization, Data curation, Formal Analysis, Investigation, Methodology, Supervision, Resources, Software, Validation, Visualization, Writing – original draft

## Conflicts of Interest

The authors declare no conflicts of interest.

## References

[1] Zhulai, D., et al. Structural and photoelectric properties of ionic liquid crystals tuned by CdS and carbon quantum dots. *Journal of Molecular Structure*. 2025, 1345, 143018. https://doi.org/10.1016/j.molstruc.2025.143018

[2] Arshad Kamran, M., Alharbi, T. Effect of Al doping on photoluminescence and conductivity of 1D CdS nanobelts synthesized by CVD for optoelectronic applications. *Journal of Science: Advanced Materials and Devices*. 2022, 7(3), 100464. https://doi.org/10.1016/j.jsamd.2022.100464

[3] Islam, M. A., et al. Comparison of Structural and Optical Properties of CdS Thin Films Grown by CSVT, CBD and Sputtering Techniques. *Energy Procedia*. 2013, 33, 203-213. https://doi.org/10.1016/j.egypro.2013.05.059

[4] Shao, Z., Zhang, Y., Cheng, J., Shi, L., Yang, X., Xiu, X. Comparing defect-assisted interfacial charge transfer in CdS/PSA and CdS/$TiO_2$NTAs nanoheterojunctions for enhanced photodegradation and biosensing. *Applied Surface Science Advances*. 2023, 18, 100464. https://doi.org/10.1016/j.apsadv.2023.100464

[5] Kolbaum, A. E., Jung, C., Jaeger, A., Libuda, L., Lindtner, O. Assessment of long-term dietary cadmium exposure in children in Germany. *Food and Chemical Toxicology*. 2024, 184, 114404. https://doi.org/10.1016/j.fct.2023.114404

[6] Tembo, M., et al. Significant reduction of blood and tissue lead and cadmium concentrations in chickens through soil remediation with biochar, phosphates, and calcined dolomite. *Journal of Hazardous Materials Advances*. 2025, 20, 100907. https://doi.org/10.1016/j.hazadv.2025.100907

[7] Mamo, S. G. Tailoring nonlinear plasmonic response of ZnSe@Ag and ZnSe@Au core-shell nanocomposites. *Hybrid Advances*. 2025, 11, 100562. https://doi.org/10.1016/j.hybadv.2025.100562

[8] Alghamdi, S. M. High-Efficiency $BaZrSe_3$/ZnSe heterojunction solar cells: A numerical simulation approach. *Results in Engineering*. 2025, 28, 107195. https://doi.org/10.1016/j.rineng.2025.107195

[9] Yoneta, M., Nanami, K., Uechi, H., Ohishi, M., Saito, H., Yoshino, K. Epitaxial growth and characterization of Cl-doped ZnSe layer by MBE. *Journal of Crystal Growth*. 2002, 237-239, 1545-1549. https://doi.org/10.1016/S0022-0248(01)02365-X

[10] He, S., Zhang, Y., Yao, H., Zuo, H., Wang, H., Feng, G. Effect of impurity distribution on optical properties of Cr-doped ZnSe nanowires. *Results in Physics*. 2023, 48, 106459. https://doi.org/10.1016/j.rinp.2023.106459

[11] Usama, M., et al. Optimizing ZnSe nanorods with La doping for device applications. *Surfaces and Interfaces*. 2024, 54, 105275. https://doi.org/10.1016/j.surfin.2024.105275

[12] Boukortt, N. E. I., Loureiro, A. G., Abushattal, A. Efficiency improvement of ultrathin CIGS solar cells. *Solar Energy*. 2024, 282, 112935. https://doi.org/10.1016/j.solener.2024.112935

[13] Vaas, T. S., et al. Light induced degradation of CIGS solar cells. *Solar Energy Materials and Solar Cells*. 2024, 275, 113036. https://doi.org/10.1016/j.solmat.2024.113036

[14] Sikder, S., Hasan, M. K., Mamur, H., Bhuiyan, M. R. A. Enhancing CIGS solar cell performance via computational simulation. *Hybrid Advances*. 2025, 10, 100460. https://doi.org/10.1016/j.hybadv.2025.100460

[15] Sharma, R., Himanshu, Patel, S. L., Chander, S., Kannan, M. D., Dhaka, M. S. Physical properties of ZnSe thin films. *Physics Letters A*. 2020, 384(4), 126097. https://doi.org/10.1016/j.physleta.2019.126097

[16] Alam, F. E., Ali, B., Arif, S. Electric field and strain mediated ZnSe. *Materials Advances*. 2024. https://doi.org/10.1039/D4MA00885E

[17] Labadi, A., Tobbeche, S., Saidani, O., Bouladame, M., Brahimi, F. Efficiency improvement of CIGS solar cells with ZnSe buffer layer and SnS BSF layer. *Micro and Nanostructures*. 2025, 206, 208257. https://doi.org/10.1016/j.micrna.2025.208257

[18] Soudagar, M. E. M., et al. Effect of electron transport layer thickness in hybrid CIGS cells. *Journal of Power Sources*. 2025, 639, 236657. https://doi.org/10.1016/j.jpowsour.2025.236657

[19] Hossain, T., et al. Tuning the bandgap of $Cd_{1-x}Zn_xS$ buffer layers for CIGS absorbers. *Superlattices and Microstructures*. 2022, 161, 107100. https://doi.org/10.1016/j.spmi.2021.107100

[20] Talbi, A., et al. Co-doped ZnS buffer layers for high-efficiency solar cells. *Chemical Physics Impact*. 2025, 11, 100942. https://doi.org/10.1016/j.chphi.2025.100942

[21] Ikhioya, I. L., et al. Influence of precursor pH on Bi-doped ZnSe synthesized electrochemically. *Applied Surface Science Advances*. 2022, 9, 100232. https://doi.org/10.1016/j.apsadv.2022.100232

[22] Lamonova, K. V., et al. ZnSe:(Cr, Fe) laser crystal matrices. *Optical Materials: X*. 2024, 22, 100321. https://doi.org/10.1016/j.omx.2024.100321

[23] Chaparro, A. M., Maffiotte, C., Gutiérrez, M. T., Herrero, J. Morphological study of CBD-ZnSe thin films. *Thin Solid Films*. 2000, 358(1), 22-29. https://doi.org/10.1016/S0040-6090(99)00704-X

[24] Somathube, S., et al. Synthesis of ZnSe QDs: optical and structural properties. *Results in Physics*. 2025, 73, 108262. https://doi.org/10.1016/j.rinp.2025.108262

[25] Dabbabi, S., Nasr, T. B., Kamoun-Turki, N. Parameters optimization of CIGS solar cell using 2D physical modeling. Results in Physics. 2017, 7, 4020-4024. https://doi.org/10.1016/j.rinp.2017.06.057

[26] Elbar, M., Tobbeche, S. Numerical simulation of CGS/CIGS single and tandem thin-film solar cells using the SILVACO-ATLAS software. Energy Procedia. 2015, 74, 1220-1227. https://doi.org/10.1016/j.egypro.2015.07.766

[27] Bouanani, B., Joti, A., Bachir Bouiadjra, F. S., Kadid, A. Band gap and thickness optimization for improvement of CIGS/CIGS tandem solar cells using SILVACO software. Optik. 2020, 204, 164217. https://doi.org/10.1016/j.ijleo.2020.164217

[28] Bechlaghem, S., Zebentout, B., Benamara, Z. The major influence of the conduction-band-offset onZn(O, S)/$CuIn_{0.7}Ga_{0.3}Se_2$ solar cells. Results in Physics. 2018, 10, 650-654. https://doi.org/10.1016/j.rinp.2018.07.006

[29] Pandey, K., et al. Suitable buffer layers for PbS quantum dot solar cells using SCAPS-1D. Optik. 2024, 298, 171593. https://doi.org/10.1016/j.ijleo.2023.171593

## Biography

**Youssou Gning** is a research professor in the Physics Department of the Faculty of Science and Technology at Iba Der THIAM University in Thiès. Dr. GNING completed a PhD thesis in Atomic and Nuclear Physics at Cheikh Anta DIOP University in Dakar. As part of this research, Dr. GNING has published on the study of resonance parameters (resonance energies and widths) of multi-electronatomic systems using variational methods. Consequently, these methods allow for a better understanding of excitation and de-excitation processes, highlighting the importance of electronic correlation phenomena in atomic systems, and exploring broader areas of the electromagnetic spectrum through the use of very intense light sources (synchrotron radiation sources and lasers). As part of expanding his research field, Dr. GNING also studies complex systems, materials as well as the field of bioenergy and biogas.

**Mamadou Lamine Samb** is an Associate Professor in Applied Physics, specialized in Electronics and Renewable Energies. He has been Head of the Physics and Chemistry Department at the University Iba Der Thiam of Thiès (UIDT) since 2020 and is currently the Scientific Coordinator of the Master's program in Physics, Chemistry, and Applications (PCA). His research focuses on numerical modeling of semiconductor devices, low-temperature thin-film transistor (TFT) simulation, and photovoltaic cell optimization. His interests also include hybrid energy systems and energy efficiency. He has extensive experience in research leadership and student supervision in electronics and renewable energies, contributing actively to capacity building, energy transition, and sustainable development in Senegal and the region.

## Research Field

**Youssou Gning:** Atomic physics, spectroscopy, photonics, Environmental and medical applications of nuclear physics, Photonics and technological developments, Semiconductor Physics and Device Electronics, Renewable energy, Numerical simulation.

**Alioune Ngom:** Semiconductor Physics and Device Electronics, Solar energy, Renewable Energy, Numerical Modeling and Simulation, Promotion of the use of renewable energies.

**Mouhamadou Sam:** Semiconductor Physics and Device Electronics, Solar energy, Renewable Energy, Numerical Modeling and Simulation, Promotion of the use of renewable energies.

**Fatma Sow:** Renewable Energy and Energy Efficiency, Photovoltaic Solar Energy, Thermal transfer, Modeling of physical systems and simulation, Energy systems diagnostics and optimization, Productive use of energy systems.

**Dimitry Diassy:** Renewable Energy and Energy Efficiency, Photovoltaic Solar Energy, Thermal transfer, Modeling of physical systems and simulation, Energy systems diagnostics and optimization, Productive use of energy systems.

**Mamadou Lamine Samb:** Nanostructuration, Semiconductor Physics and Device Electronics, Photovoltaic Solar Energy, Renewable Energy and Hybrid Systems, Energy Efficiency and System Optimization, Numerical Modeling and Simulation, Sustainable Development and Renewable Energy Education.

**Ahmed Mohamed-Yahya:** Renewable Energy and Energy Efficiency, Photovoltaic Solar Energy, thermal transfer, modeling of physical systems and simulation, Energy systems diagnostics and optimization, Productive use of energy systems.